THE BELL SYSTEM
TECHNICAL JOURNAL

VOLUME XLII SEPTEMBER 1963 NUMBER 5

Phase-Lock Loop Design for Coherent Angle-Error Detection in the *Telstar* Satellite Tracking System

By W. L. NELSON

(Manuscript received January 14, 1963)

The function of the angle-error detector is to provide pointing-error signals to the ground antenna control system, which allows operation in the autotrack mode once the satellite beacon has been acquired. The limitations on the accuracy of this system imposed by noise, phase jitter and Doppler effects are evaluated and the optimum design in terms of minimum mean-square error is developed. Design examples are given for both the horn-reflector antenna autotrack system and the precision tracker antenna system.

I. INTRODUCTION AND SUMMARY

To insure the acquisition and accurate tracking of the Telstar communication satellites, a sequence of tracking modes is provided at the ground stations in Andover, Maine and Pleumeur-Bodou, France.[1]

Initial pointing directions to both the precision tracker[2] and the horn-reflector antennas are provided from orbital data appropriately processed and up-dated for each satellite pass. Once the precision tracker acquires and tracks the satellite, the horn-reflector antenna can use the pointing directions received from the precision tracker control system to acquire the satellite beacon signal in its narrow beamwidth. Finally, the autotrack system[3] provides closed-loop automatic control of the horn-reflector antenna using error signals derived from the satellite beacon.*

* After orbital data becomes sufficiently accurate, it is possible for the horn antenna to acquire the satellite from initial pointing directions and then go directly into the autotrack mode without using the precision tracker.

The detection of these error signals is accomplished in the system described in this paper. The inputs to this system are obtained by means of a mode separation technique[3] in the waveguide of the horn antenna, one mode having a peak amplitude on target, the other having a null, similar to the sum and difference signals in conventional monopulse tracking systems. The characteristics of these input signals and noise are discussed in Section II. An analysis of the phase-lock detection scheme which converts these inputs into the desired antenna pointing-error signals is given in Section III. The accuracy of these pointing-error signals is shown to be critically dependent upon the degree of phase coherence achieved by the phase-lock loop, which is discussed in Section IV. The design of the phase-lock loop to minimize the mean-square phase error in the output signals is considered in Section V.

In Section VI a numerical example is given for the optimum design of the phase-lock detector in the vernier autotrack system. Since the precision tracker also uses essentially the same angle-error detection scheme, a parallel design of this system is included for comparison.

II. INPUT SIGNAL AND NOISE CHARACTERISTICS

The function of the angle error detector is to develop electrical error signals proportional to the pointing angle error, β, between the antenna boresight and the actual satellite position. The expressions for the desired output error signals are

$$\begin{aligned} \epsilon_x &= \beta \cos \varphi \\ \epsilon_y &= \beta \sin \varphi \end{aligned} \tag{1}$$

where x and y are Cartesian coordinates in the plane normal to the antenna boresight (electrical) and φ is the angle which the projection on the x-y plane of the radius vector, R, to the satellite makes with the x-axis, (see Fig. 1).

The information on the parameters β and φ necessary for the error signals (1) is contained in the amplitude and phase, respectively, of the difference channel received signal relative to the sum channel* received signal. For a pointing error, β, which is within the beamwidth

* The designations "difference" and "sum" channels are carried over from conventional monopulse usage. For the autotrack system, these terms should be "TM_{10}" and "TE_{11}" channels, respectively. This analysis is applicable to a single plane in conventional (linearly polarized) monopulse if the angle φ is taken to be 0 or 180 degrees.

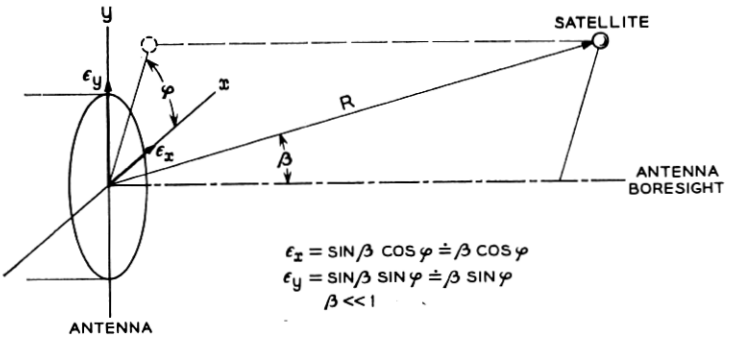

Fig. 1 — Pointing error, β, and the angle φ in the x-y plane which determine the orthogonal error signals: $\epsilon_x = \beta \cos \varphi$; $\epsilon_y = \beta \sin \varphi$.

of the sum pattern (the TE_{11} mode pattern in the horn-reflector antenna), the received signals in the sum and difference channels can be expressed as[3]

$$\begin{aligned} e_s(t) &= E_s(R,\beta) \cos (\omega_b t + \theta_i(t)) + N_s(t) \\ e_d(t) &= \eta\beta E_s(R,\beta) \cos (\omega_b t + \theta_i(t) + \varphi) + N_d(t) \end{aligned} \tag{2}$$

where

ω_b = $2\pi \times$ frequency of satellite beacon transmitter,
R = range of the satellite,
$E_s(R,\beta)$ = sum channel signal amplitude,
η = difference channel relative sensitivity,

$$= \frac{1}{E_s} \left| \frac{\Delta E_d}{\Delta \beta} \right|_{\beta=0}$$

and

$\theta_i = \theta_s(t) + \theta_n(t)$, is the signal phase relative to a reference phase,
$\theta_r = 0$, plus a random phase fluctuation, $\theta_n(t)$, discussed below.

$N_s(t)$ and $N_d(t)$ are the thermal noise components at the inputs of the sum and difference channels, respectively, whose one-sided power-spectral densities are assumed identical and equal to

$$\Phi_N = kT_{eq} \text{ watts/cps} \tag{3}$$

where

$k = 1.38 \times 10^{-23}$ watt-sec/°K
T_{eq} = equivalent receiver noise temperature, °K.

The random phase fluctuation, $\theta_n(t)$, results from the frequency instability of the various oscillators in the system, principally the beacon oscillator in the satellite, since elaborate frequency stabilizing techniques are not feasible from weight and space considerations. The one-sided spectral density of the resultant phase fluctuation can be expressed as

$$\Phi_\theta = \frac{2}{\tau_{ce}\omega^2} \text{ rad}^2/\text{cps} \tag{4}$$

where

τ_{ce} = equivalent coherence time of the system oscillators.[4]

For the purpose of this analysis, the thermal noise terms in (2) will be represented by the usual in-phase and quadrature notation[4,5]

$$N(t) = X(t) \cos (\omega_b t + \theta_i) + Y(t) \sin (\omega_b t + \theta_i)$$

where $X(t)$, $Y(t)$ = independent Gaussian random voltages with one-sided power spectral density, $2\Phi_N$, with Φ_N given in (3).*

With identical receivers in the sum and difference channels which amplify the signals (2) by a factor K_0 and reduce the center frequency from ω_b to an intermediate frequency, $\omega_i = 2\pi \times 60$ mc, the input to the sum and difference channels of the coherent angle-error detector can be represented by

$$\begin{aligned} e_{s_i}(t) &= K_0[E_s(R,\beta) \cos (\omega_i t + \theta_i(t)) \\ &\quad + X_s(t) \cos (\omega_i t + \theta_i(t)) \\ &\quad + Y_s(t) \sin (\omega_i t + \theta_i(t))] \\ e_{d_i}(t) &= K_0[\eta\beta E_s(R,\beta) \cos (\omega_i t + \varphi + \theta_i(t)) \\ &\quad + X_d(t) \cos (\omega_i t + \theta_i(t)) \\ &\quad + Y_d(t) \sin (\omega_i t + \theta_i(t))] \end{aligned} \tag{5}$$

where $X_s(t)$, $X_d(t)$, $Y_s(t)$, $Y_d(t)$ have identical one-sided power density spectra $2\Phi_N$ band-limited by the IF bandwidth, B_{IF}, hence have mean-square expected values, $\overline{X^2} = \overline{Y^2} = \Phi_N B_{IF}$.

III. LINEAR ANALYSIS OF COHERENT ANGLE-ERROR DETECTION SYSTEM

A block diagram of the coherent angle-error detection system is given in Fig. 2. The coherence between the input error signal and the

* The fluctuation of θ_i due to Doppler and random phase effects is assumed to have negligible effect on the power spectral densities of $X(t)$ and $Y(t)$.

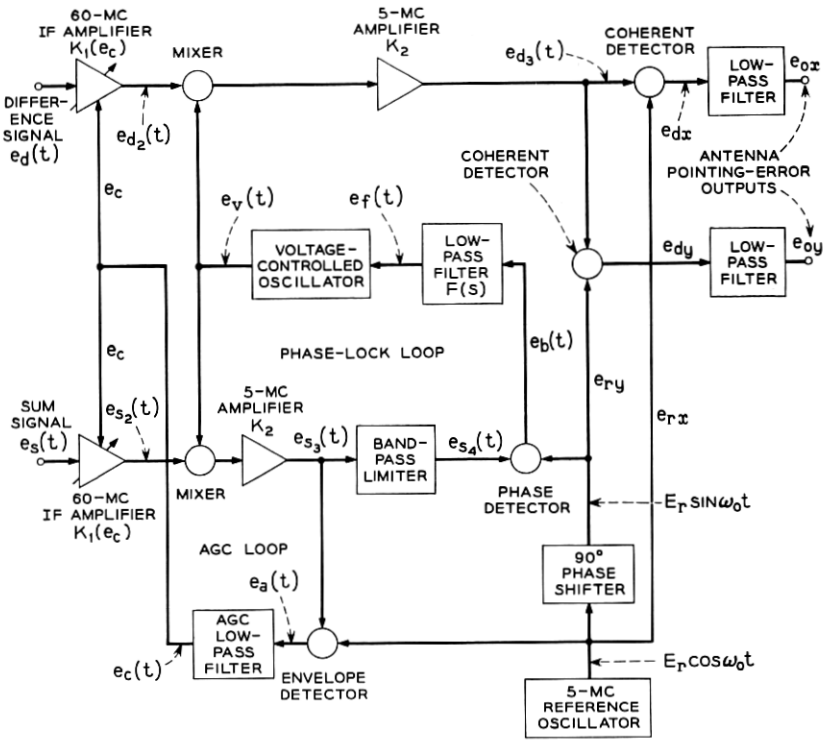

Fig. 2 — Coherent angle-error detection system block diagram.

local reference signal is achieved through the action of the phase-lock loop. The mixers and detectors indicated by circles in Fig. 2 are assumed to be ideal multipliers with unity gain. The AGC action is assumed to respond perfectly to variations in the sum channel signal level, so the gain of the 60-mc IF amplifiers in both channels can be expressed as

$$K_1(e_c) = \frac{E}{E_s(R,\beta)}, \qquad E = \text{constant}. \tag{6}$$

Using (5) and (6), the input to the mixers in each channel in Fig. 2 can be written

$$e_{s_2}(t) = K_0 E \left[\cos(\omega_i t + \theta_i) + \frac{X_s}{E_s} \cos(\omega_i t + \theta_i) + \frac{Y_s}{E_s} \sin(\omega_i t + \theta_i) \right] \tag{7a}$$

$$e_{d_2}(t) = K_0 E \left[\eta\beta \cos(\omega_i t + \varphi + \theta_i) + \frac{X_d}{E_s} \cos(\omega_i t + \theta_i) + \frac{Y_d}{E_s} \sin(\omega_i t + \theta_i) \right] \tag{7b}$$

where the dependence of E_s on R and β and the time dependence of θ_i, X, and Y is understood, but not indicated explicitly in (7) and the subsequent analysis, to simplify the equations.

The other input to the mixers is the output of the voltage-controlled oscillator (VCO) in the phase-lock loop, which has the form

$$e_v(t) = E_v \cos(\omega_v t + \theta_v) \tag{8}$$

where $\omega_v = 2\pi \times 65$ mc and $\theta_v = \theta_v(t)$ is the instantaneous phase of the VCO output, determined by the operation of the feedback loop in the sum channel, which is discussed in the next section. Multiplying (7) and (8) and taking only the low-frequency (5-mc) components gives at the outputs of the 5-mc IF amplifier in the sum and difference channels (see Fig. 2)

$$\begin{aligned} e_{s_3}(t) &= E_3 \left[\cos(\omega_o t - \theta_i + \theta_v) + \frac{X_s}{E_s} \cos(\omega_o t - \theta_i + \theta_v) - \frac{Y_s}{E_s} \sin(\omega_o t - \theta_i + \theta_v) \right] \\ e_{d_3}(t) &= E_3 \left[\eta\beta \cos(\omega_o t - \varphi - \theta_i + \theta_v) + \frac{X_d}{E_s} \cos(\omega_o t - \theta_i + \theta_v) - \frac{Y_d}{E_s} \sin(\omega_o t - \theta_i + \theta_v) \right] \end{aligned} \tag{9}$$

where

$$E_3 = \tfrac{1}{2} K_0 K_2 K_m E E_v \qquad K_m = \text{mixer gain, (volts)}^{-1}$$

$$\omega_0 = \omega_v - \omega_i = 2\pi \times 5 \text{ mc}.$$

The difference channel voltage, $e_{d_3}(t)$, is applied to the coherent detectors. The other input to these detectors comes from the 5-mc reference oscillator which produces signals

$$\begin{aligned} e_{r_x} &= E_r \cos \omega_0 t \\ e_{r_y} &= E_r \sin \omega_0 t \end{aligned} \tag{10}$$

for the detection of the desired x and y error components given in (1). The phase of these signals is the reference phase, $\theta_r = 0$.

The low-pass filters following the coherent detectors pass only the baseband components of the products $(e_{d_3} \cdot e_{r_x})$ and $(e_{d_3} \cdot e_{r_y})$. Using (9) and (10) these baseband components are

$$\begin{aligned} e_{dx} &= A\left[\eta\beta \cos(\varphi + \theta_i - \theta_v) + \frac{X_d}{E_s}\cos(\theta_i - \theta_v)\right. \\ &\quad \left. + \frac{Y_d}{E_s}\sin(\theta_i - \theta_v)\right] \\ e_{dy} &= A\left[\eta\beta \sin(\varphi + \theta_i - \theta_v) + \frac{X_d}{E_s}\sin(\theta_i - \theta_v)\right. \\ &\quad \left. - \frac{Y_d}{E_s}\cos(\theta_i - \theta_v)\right] \end{aligned} \tag{11}$$

where

$$A = \tfrac{1}{2}K_d E_3 E_r = \text{channel amplification factor}$$

$$K_d = \text{detector gain, (volts)}^{-1}.$$

If the phase-lock loop is tracking properly, the phase of the VCO output, θ_v, will follow closely the phase of the input, θ_i. Assuming that the rms value of $(\theta_i - \theta_v)$ is small compared to 1 radian, then the following approximations hold with high probability*

$$\sin(\theta_i - \theta_v) \doteq (\theta_i - \theta_v) \ll 1$$

$$\cos(\theta_i - \theta_v) \doteq 1$$

and the coherent detector outputs (11) can be expressed in the approximate form

$$\begin{aligned} e_{dx} &\doteq A\eta\beta\cos\varphi - A\left(\eta\beta\sin\varphi - \frac{Y_d}{E_s}\right)(\theta_i - \theta_v) + A\frac{X_d}{E_s}, \\ e_{dy} &\doteq A\eta\beta\sin\varphi + A\left(\eta\beta\cos\varphi + \frac{X_d}{E_s}\right)(\theta_i - \theta_v) - A\frac{Y_d}{E_s}. \end{aligned} \tag{12}$$

The first term in each of the expressions in (12) is the desired error component, given in (1), amplified by the total difference channel gain, $A\eta$. The second term represents the perturbation due to the lack of perfect phase coherence, while the third term represents the contribution of thermal noise in the net noise bandwidth of the difference channel.

* The validity of these assumptions is discussed in the next section.

The achievement of good phase coherence in the detector outputs (12) over the expected range of satellite tracking conditions is the objective of the phase-lock loop analysis and design described in the following sections.

IV. PHASE-LOCK LOOP ANALYSIS

The coherent detection of the control error signals depends on the performance of the phase-lock loop in the sum channel (see Fig. 2). The loop must be capable of following the change of phase of the input signal due to frequency instability of the source and Doppler shift and also discriminate against random phase fluctuations caused by thermal noise. These requirements are somewhat contradictory, the former requiring a wide loop bandwidth and the latter requiring a narrow loop bandwidth. Proper design of the phase-lock loop must therefore be based on the best compromise of these requirements consistent with the expected variation of the signal phase and the expected random phase fluctuation.

The sum channel voltage, $e_{s_3}(t)$ at the input to the bandpass limiter is given in (9). The effect of the limiter can be closely approximated as multiplying this voltage by a limiter suppression factor, α, which increases from 0 to 1 as the signal-to-noise ratio at the limiter input increases from 0 to ∞. This limiter action is discussed in Appendix A.

The limiter output voltage, $e_{s_4}(t) = \alpha e_{s_3}(t)$ is applied to the phase detector in the sum channel, together with the reference signal, e_{r_y}, given in (10). The baseband component of the phase detector output is therefore

$$e_b(t) = (e_{r_y} \cdot \alpha e_{s_3})_{\text{baseband}}$$

or, from (9) and (10)

$$e_b(t) = \alpha A\left[\left(1 + \frac{X_s}{E_s}\right)\sin(\theta_i - \theta_v) - \frac{Y_s}{E_s}\cos(\theta_i - \theta_v)\right]. \quad (13)$$

To develop an approximate linear model for the phase-lock loop, the following two assumptions are made:

(*i*) the phase error $(\theta_i - \theta_v)$ is sufficiently small to permit the approximations $\sin(\theta_i - \theta_v) \doteq \theta_i - \theta_v$, $\cos(\theta_i - \theta_v) \doteq 1$, and

(*ii*) the noise component, $X(t)$, is assumed small in the rms sense compared to the signal amplitude, E_s.

Using these assumptions, the phase detector output (13) can be written in the approximate form

$$e_b(t) \doteq \alpha A\left[\theta_i(t) - \theta_v(t) - \frac{Y_s(t)}{E_s}\right]. \quad (14)$$

The low-pass filter passes the baseband component $e_b(t)$, producing a voltage $e_f(t)$ which causes the frequency of the VCO to vary from the center frequency, $\omega_v = 2\pi \times 65$ mc, with a proportionality constant, K_v radians per second per volt. The instantaneous phase of the VCO output is therefore

$$\theta_v(t) = K_v \int e_f(t)\, dt, \text{ radians.}$$

The transfer function of the VCO over the range in which this proportionality holds is then

$$\frac{\theta_v(s)}{e_f(s)} = \frac{K_v}{s}. \tag{15}$$

For a phase-lock loop which is stable over a large range of loop gain variations and which has zero steady-state phase error for a phase ramp input (step frequency change) the low-pass filter should have a transfer function of the form

$$F(s) = \frac{e_f(s)}{e_b(s)} = \frac{1 + \tau s}{s}. \tag{16}$$

This transfer function has been shown[6] to yield optimum loop performance for phase ramp inputs in the presence of white noise, where the performance measure is the mean-square error caused by noise plus the integrated-squared transient error to the ramp input.

The transfer function (16) can be closely approximated by the operational amplifier circuit shown in Fig. 3, which has the transfer function

$$F(s) = -\mu \frac{1 + R_2 C s}{1 + \mu R_1 C s} \tag{17}$$

where $-\mu$ is the amplifier gain under load without feedback. The

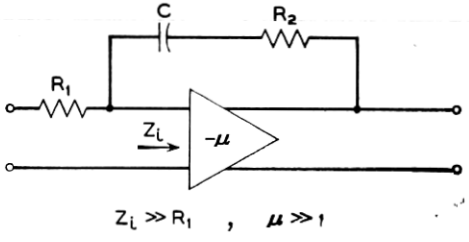

Fig. 3 — Operational amplifier low-pass filter circuit.

assumptions made in deriving (17) are that the input impedance, Z_i, of the amplifier is very large compared to R_1 and that $\mu \gg 1$ (typically 10^6) in the low-frequency range. With $R_1C = 1$ second and μ of the order of 10^6, the transfer function (17) reduces to

$$F(s) \doteq -\frac{1 + R_2Cs}{s} \tag{18}$$

which is the desired form (16), with $R_2C = \tau$. The negative sign in (18) is incidental provided the sign of the total gain around the loop gives negative feedback.

Using (14), (15), and (16), the linear equivalent block diagram for the phase-lock loop is shown in Fig. 4. The objective of the design is to minimize the mean-square value of the random phase error, $\theta_e(t) = \theta_i(t) - \theta_v(t)$, consistent with the requirements on the dynamic tracking capability of the loop.

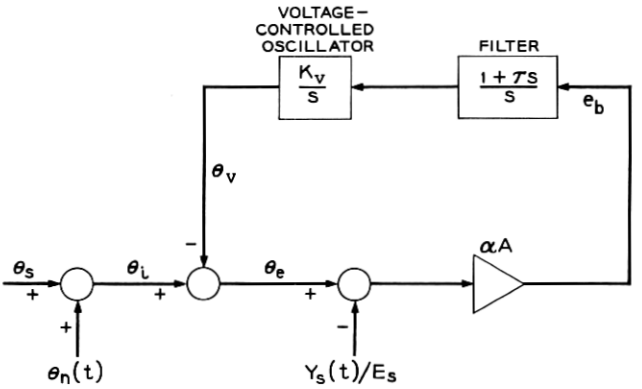

Fig. 4 — Block diagram of phase-lock loop based on linear analysis.

The total transfer function around the loop is

$$G(s) = \frac{\theta_v(s)}{\theta_e(s)} \doteq \alpha K \frac{1 + \tau s}{s^2} \tag{19}$$

where $K = AK_v$. [If R_1C is not unity, as was assumed in (18), then $K = AK_v/R_1C$.]

For the analysis of the phase error, θ_e, due to the noise sources $\theta_n(t)$ and $Y_s(t)$, we let the signal phase θ_s be zero and obtain from Fig. 4 the transfer function for θ_e in terms of $G(s)$ in (19)

$$\theta_e(s) = \left[\frac{1}{1 + G(s)}\right]\theta_n(s) + \left[\frac{G(s)}{1 + G(s)}\right]\frac{Y_s(s)}{E_s}. \tag{20}$$

Since the one-sided power density spectrum of $\theta_n(t)$ is Φ_θ, given in (4), and that of $Y_s(t)/E_s$ is $2\Phi_N/E_s^2$ where Φ_N is given in (3), and since they are uncorrelated random variables, the one-sided power density spectrum of the random phase error, θ_e, is

$$\Phi_{\theta_e} = \left| \frac{1}{1 + G(j\omega)} \right|^2 \frac{2}{\tau_{ce}\,\omega^2} + \left| \frac{G(j\omega)}{1 + G(j\omega)} \right|^2 \frac{2\Phi_N}{E_s^2}. \tag{21}$$

The mean-square value of this random phase error is then, from (19), (21) and integral tables[7]

$$\sigma_e^2 = \int_0^\infty \Phi_{\theta_e} \frac{d\omega}{2\pi} = \frac{1}{\tau_{ce}} \left(\frac{1}{2\alpha K \tau} \right) + \frac{2\Phi_N}{E_s^2} \left(\frac{\alpha K \tau}{4} + \frac{1}{4\tau} \right), \text{ rad}^2. \tag{22}$$

This expression for the mean-square phase error can be written in terms of the undamped natural frequency, ω_n, and the damping ratio, ζ, of the phase-lock loop, as

$$\sigma_e^2 = \frac{1}{4\zeta\omega_n\,\tau_{ce}} + \frac{2\Phi_N}{E_s^2}\,\omega_n \left(\frac{1 + 4\zeta^2}{8\zeta} \right) \tag{23}$$

since $\omega_n = \sqrt{\alpha K}$, and $2\zeta = \tau\sqrt{\alpha K}$.

The proper operation of the phase-lock loop depends upon the magnitude of the phase error remaining less than $\pi/2$ radians. For the phase error due to random fluctuations we can require only that the probability of its magnitude exceeding $\pi/2$ radians be very small. A criterion for this which has been chosen[4,8] as a realistic measure of the threshold of the phase-lock loop is that the mean-square value of the total phase error be restricted by

$$\sigma_e^2 \leqq \tfrac{1}{8} \text{ rad}^2. \tag{24}$$

For a normally distributed random phase error with zero mean and variance σ_e^2, this criterion implies that the probability of exceeding $\pi/2$ is exceedingly small (about 10^{-5}). This criterion also gives validity to the first assumption made above in obtaining the linear model of the phase-lock loop, namely that $\sin\theta_e \doteq \theta_e$ and $\cos\theta_e \doteq 1$. The error in these approximations is quite small provided

$$|\,\theta_e\,| \leqq 0.57 \text{ radian}$$

which holds with approximately 90 per cent probability when the condition (24) is satisfied.

The second assumption made above for the linear model is not strictly justified in the region of threshold, where the signal-to-noise ratio in the 3-kc bandwidth at the phase detector input will typically be less than

unity. However, comparison studies with a digital computer simulation[9] which was implemented for the angle-error detector in the precision tracker system have indicated that the linear model estimate of the mean-square phase error (23) is sufficiently accurate even in the vicinity of threshold to justify its use for the analytical design optimization of the phase-lock loop. The digital computer baseband model of the phase-lock loop includes the in-phase noise term as well as the quadrature noise term in (13), and the sine and cosine operations of the phase detector (see Ref. 9). A comparison of the computer simulation data with the linear analysis data for the design examples considered in Section VI is given at the end of that section.

An important parameter in the phase-lock loop analysis is the effective noise bandwidth, B_L, of the loop, defined by

$$B_L = \int_0^\infty \left| \frac{G(s)}{1 + G(s)} \right|^2 df.$$

The loop noise bandwidth for the system under consideration has already been evaluated in the second terms of (22) and (23), namely

$$B_L = \frac{\alpha K \tau}{4} + \frac{1}{4\tau} = \omega_n \left(\frac{1 + 4\zeta^2}{8\zeta} \right) \tag{25}$$

which increases with the limiter suppression factor α and hence increases with the signal-to-noise power ratio at the limiter input. This is the desired adaptive feature which the limiter provides in the phase-lock loop operation, since for small S/N (long-range condition) the loop bandwidth is small, decreasing the mean-square error due to thermal noise, while for large S/N (short-range condition) the loop bandwidth is large, providing improved phase tracking accuracy for the greater Doppler frequency rate of change occurring at short range.

The Doppler frequency variation as a function of time is approximated by a frequency "ramp" input having a constant slope of magnitude $\dot{\omega}$ for a duration T_d, as indicated in Fig. 5. Since this approximate function represents a somewhat more difficult variation for the loop to track than the actual Doppler variation, the evaluation of the loop tracking accuracy and transient behavior based on the approximate input should serve as a conservative basis for design.

Neglecting the thermal noise terms in (13), the phase detector output reduces to

$$e_b(t) = \alpha A \sin [\theta_i(t) - \theta_v(t)] \text{ volts} \tag{26}$$

where $\theta_i(t) = \frac{1}{2}\dot{\omega}t^2$ is the phase input corresponding to the frequency

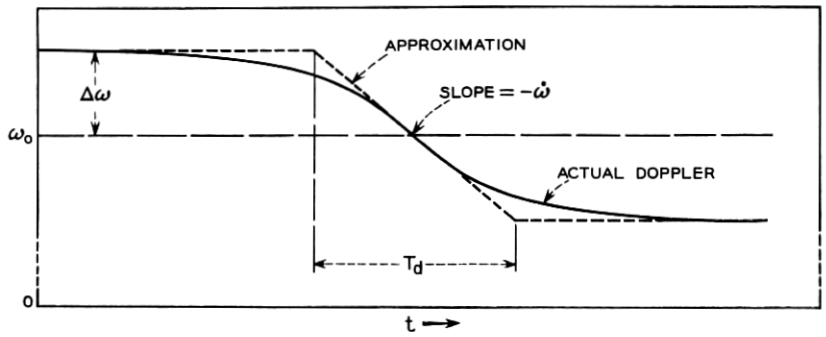

Fig. 5 — Typical Doppler frequency variation and piecewise linear approximation.

"ramp" input discussed above. Since this output is bounded in magnitude by $\pm A$ volts, the low-pass filter which follows the phase detector should have a linear input dynamic range of at least this magnitude. In addition, the voltage-controlled oscillator should have a linear frequency range at least as large as the expected maximum Doppler shift. With these two design requirements satisfied, the only essentially nonlinear element in the phase-lock loop circuit is the phase detector (see Fig. 6a).

An analysis of the response of this nonlinear circuit to a frequency "ramp" input is given in Appendix B. From this analysis it is concluded that for adequate phase-lock tracking of the Doppler shift, the loop gain should satisfy the condition

$$\alpha K > 2\dot{\omega}_{\max} \tag{27}$$

where $\dot{\omega}_{\max}$ is the maximum Doppler rate in rad/sec^2.

When condition (27) is satisfied, the steady-state phase error due to this Doppler rate will not exceed $\pi/6$ radian (see Appendix B), and the loop response will closely approximate that of the linear second-order circuit, shown in Fig. 6(b). For this circuit with the input $\theta_i(t) = \frac{1}{2}\dot{\omega}t^2$, the Laplace transform of the phase error is

$$\theta_e(s) = \frac{\dot{\omega}}{s[s^2 + 2\zeta\omega_n s + \omega_n^2]}$$

where, as before, $\omega_n = \sqrt{\alpha K}$, $2\zeta = \tau\sqrt{\alpha K}$, and $K = AK_v$. The time response of this type of linear second-order system is thoroughly discussed in elementary texts on linear circuits or control system theory.*

* See, for example, Ref. 10.

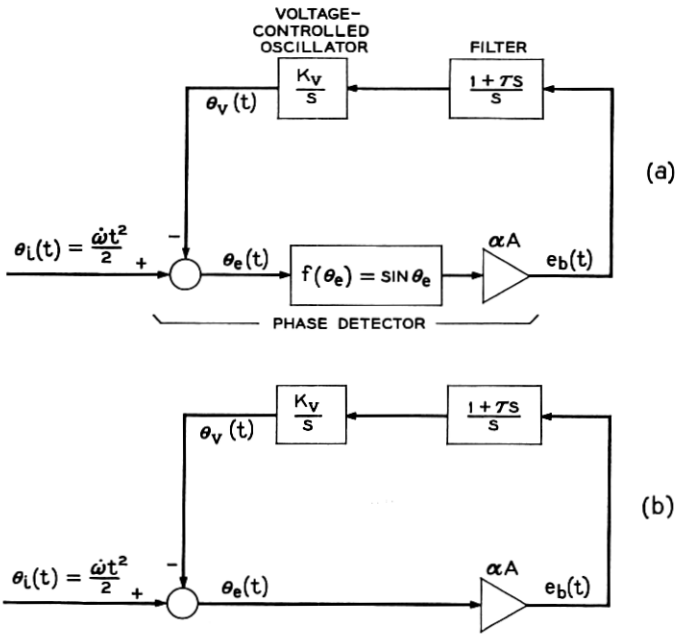

Fig. 6 — Phase-lock loop circuits for Doppler-shift analysis: (a) equivalent circuit including nonlinearity of phase detector; (b) approximate linear circuit, valid for $|\theta_e| \leqq \pi/6$ radian.

The two per cent settling time* for the transient of the phase error is approximately

$$T_s \doteq \frac{8\zeta}{\omega_n} = 4\tau \text{ seconds} \tag{28}$$

for the overdamped case ($\zeta > 1$). This also serves as a good approximation of the duration of the transient for the underdamped case in the range $0.7 < \zeta < 1$.

V. PHASE-LOCK LOOP DESIGN

The design procedure which will be followed is first to ascertain the system requirements necessary for minimum acceptable performance and second to optimize the performance within the range of parameter adjustment available to the designer.

* Defined as the time required for the transient response to settle down to within two per cent of the steady-state value. See Ref. 10.

The primary factors external to the phase-lock loop which affect its performance capability are:

(*i*) *The equivalent coherence time,* τ_{ce}, of the input signal, which characterizes the random frequency fluctuations of the various system oscillators which affect the instantaneous frequency of the signal into the phase-lock loop. The coherence time should be made as large as possible, but is primarily limited by the frequency stability achievable in the small satellite transmitter and hence will be considered a fixed parameter not available for phase-lock loop design adjustment.

(*ii*) *The noise-to-signal power ratio* at the input to the phase-lock loop. Since this ratio varies with the range of the satellite and with the IF bandwidth preceding the loop, it is desirable to characterize the relative "noisiness" of the system independent of range and bandwidth variations. The thermal noise power is given by

$$N = \Phi_N B_{IF} = kT_{eq}B_{IF} \text{ watts}$$

while the average signal power is[11,12]

$$S = \frac{E_s^2}{2} = \frac{P_T G_T A_r}{4\pi R^2} \text{ watts}$$

where

P_T = transmitter power, watts,
G_T = transmitter antenna gain,
R = transmitter to receiver range, and
A_r = effective area of receiving antenna (same units as R^2).

The noise-to-signal power ratio can then be expressed as

$$\frac{N}{S} = \frac{2\Phi_N}{E_s^2} B_{IF} = \left(\frac{4\pi k T_{eq}}{P_T G_T A_r}\right) R^2 B_{IF} . \tag{29}$$

The factors in parenthesis in (29) are constant* characteristics of the satellite-ground system and will be represented by a single constant called the "receiver noise index," denoted by the symbol k_r, and having the units of seconds/(distance)^2. Then,

$$\frac{N}{S} = \frac{2\Phi_N}{E_s^2} B_{IF} = k_r R^2 B_{IF} . \tag{30}$$

The noise index, k_r, is taken as the second fixed parameter† of the

* The transmitter antenna gain, G_T, will not actually be constant unless the radiation pattern is uniform or the satellite is properly attitude controlled. It is assumed essentially constant in this study.

† From (30) it is apparent that the receiver noise index, k_r, corresponds to the unit bandwidth noise-to-signal power ratio in the receiver when the satellite is at unit distance from the receiver.

external system affecting loop design.

*(iii) The satellite orbit characteristics.** The orbit characteristics affect the performance capability of the phase-lock loop as follows: First, the maximum and minimum communication range will determine the variation of the noise-to-signal ratio as shown in (30). Second, the maximum range rate, $\dot{R}_{\max}$, will determine the maximum Doppler shift

$$|\Delta\omega|_{\max} = \frac{\omega_b |\dot{R}|_{\max}}{c} \text{ rad/sec} \tag{31}$$

where

$\omega_b = 2\pi \times$ satellite beacon frequency, and
$c =$ velocity of light.

Finally, the maximum range acceleration, $\ddot{R}_{\max}$, will determine the maximum Doppler rate

$$\dot{\omega}_{\max} = \frac{\omega_b \ddot{R}_{\max}}{c} \text{ rad/sec}^2 . \tag{32}$$

Since the maximum $\dot{\omega}$ occurs at the range of closest approach for all possible satellite passes, the limiter suppression factor α will be at its maximum value, giving the largest loop gain, $\alpha_{\max} K$. From (27), the basic lower limit on the fixed loop gain constant, K, is then

$$K > \frac{2\dot{\omega}_{\max}}{\alpha_{\max}} \sec^{-2} . \tag{33}$$

The total mean-square error due to random fluctuations in the system is given by (22) or (23). Using (25) and (30), the mean-square error can be expressed as

$$\sigma_e^2 = \frac{1 + (1/4\zeta^2)}{8\tau_{ce} B_L} + k_r R^2 B_L , \text{ rad}^2 . \tag{34}$$

The second term in (34), due to thermal noise in the system characterized by k_r, increases with the square of the range. This increase is somewhat offset by the reduction of the loop bandwidth, B_L, which decreases approximately as the first power of the range. This reduction of B_L, however, increases the mean-square error due to random phase fluctuations of the signal, given by the first term in (34). Hence, the total mean-square error will be maximum at the longest range condition.

* Derivation of pertinent orbit characteristics is given in Appendix C.

From (24), a requirement which the loop design must satisfy is therefore given by

$$(\sigma_e^2)_{R=R_{\max}} \leqq \tfrac{1}{8} \text{ rad}^2. \tag{35}$$

As a function of B_L, the minimum possible value of σ_e^2 is, from (34)

$$\min \sigma_e^2 = R\left[\frac{k_r}{2\tau_{ce}}\left(1 + \frac{1}{4\zeta^2}\right)\right]^{\frac{1}{2}} \tag{36}$$

when

$$B_L = \text{opt } B_L = \frac{1}{R}\left(\frac{1 + (1/4\zeta^2)}{8\tau_{ce}k_r}\right)^{\frac{1}{2}}. \tag{37}$$

It is apparent from (36) that unless

$$\frac{k_r R_{\max}^2}{\tau_{ce}} < \frac{1}{32} \tag{38}$$

the condition (35) cannot be satisfied for any values of loop bandwidth and damping ratio, or equivalently for any values of loop gain, αK, and time constant, τ. This corresponds to the minimum signal power condition given by Develet.[4]

The two basic design requirements which the external system imposes upon the phase-lock loop design are given by the inequalities (33) and (38). The first requirement does not appear critical, since for satellite communication systems the value of $\dot{\omega}_{\max}$ is unlikely to exceed about 2×10^4 rad/sec^2 (see Appendix C). Since $\alpha_{\max} \doteq 1$, condition (33) requires that

$$K > 4 \times 10^4 \text{ sec}^{-2}$$

while values of K on the order of ten times this lower limit are achievable in present phase-lock loop designs.

The second requirement, (38), is more critical, since it depends entirely upon the fixed parameters of the external system. If the inequality (38) is not satisfied, either the system noise index must be decreased or the coherence time of the satellite transmitter must be increased before satisfactory operation of the phase-lock loop can be achieved at maximum range. When this requirement is satisfied, the optimum loop design with respect of the total mean-square error is achieved by making the loop bandwidth equal to the optimum value, given by (37), and by making the damping ratio, ζ, as large as is consistent with satisfactory transient response of the loop.

Fig. 7 depicts in graphical form the design requirements discussed

above. For a given value of

$$\tau_{ce}' = \frac{\tau_{ce}}{1 + (1/4\zeta^2)} \tag{39}$$

the contour of $\sigma_e^2 = \frac{1}{8}$ rad^2 is given as a function of $k_r R^2$ and the loop bandwidth B_L. Within this contour the mean-square error is less than the threshold value of $\frac{1}{8}$ rad^2 and has its minimum possible value for a given $k_r R^2$ on the dashed line associated with each contour. The vertical line defined by $k_r R^2 = k_r R_{\max}^2$ must intersect the contour for the appropriate value of τ_{ce}' in order for satisfactory loop design to be achieved. If this critical requirement is satisfied, then the optimum design is given by adjusting the loop bandwidth, B_L, to equal the value obtained from the dashed line within the contour at the particular value of $k_r R^2$.

The input-adaptive adjustment of B_L by means of the limiter sup-

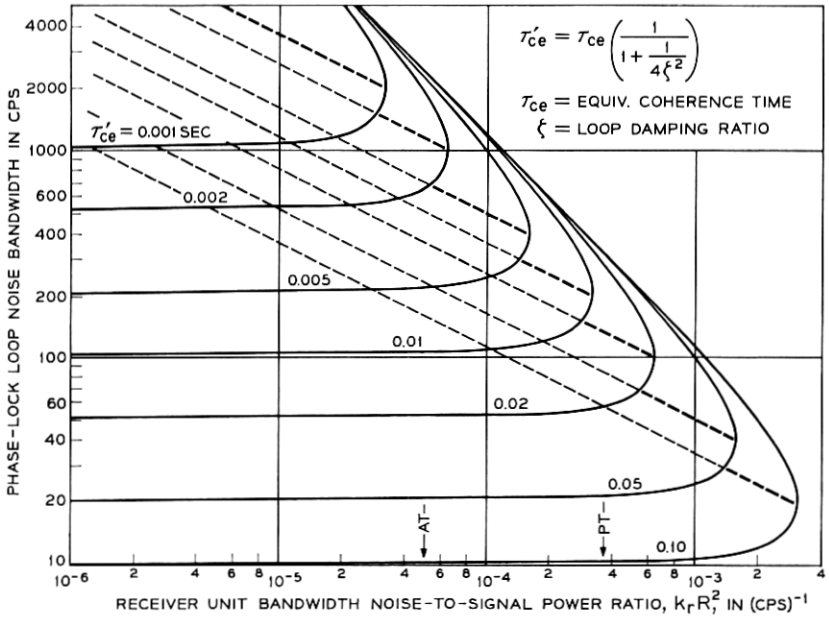

Fig. 7 — Phase-lock loop threshold contours. Inside the contour for a particular τ_{ce}' the mean-square phase error, σ_e^2, is less than the threshold value of 0.125 rad^2, and has its minimum value for a given $k_r R^2$ on the dashed line associated with the contour. Indicated on the abscissa are the expected maximum values of $k_r R^2$ for the autotrack and the precision tracker.

pression factor, α, can approximate this optimum adjustment of B_L. The optimum B_L, given by (37), varies inversely with the range, R. The actual value of B_L, given by (25), varies directly with α, but α itself varies inversely with R, as shown in Appendix A.

Before the optimum bandwidth can be determined from (37) or Fig. 7, the value of ζ at maximum range must be chosen. As was pointed out at the end of Section IV, the settling time of the loop is approximately 4τ seconds. If T_M denotes the maximum tolerable settling time, then this requires that $4\tau \leqq T_M$. This also places an upper limit on ζ when the loop bandwidth, B_L, is fixed at the optimum value (37), since, from (25), B_L and ζ are related to τ as follows

$$B_L = \frac{1}{4\tau}(4\zeta^2 + 1).$$

To satisfy the maximum settling time restriction, then

$$4\tau = \frac{4\zeta^2 + 1}{B_L} \leqq T_M \tag{40}$$

which implies that ζ cannot be arbitrarily increased while holding B_L fixed at the optimum B_L. Using (37), (39) and (40), the upper bound on ζ when $B_L = \text{opt } B_L$ can be expressed in terms of T_M and the external system parameters as

$$\zeta^2 \leqq \zeta_M{}^2 \equiv \tfrac{1}{8}\left[\left(\frac{T_M{}^2}{2\tau_{ce}k_rR^2} + 1\right)^{\frac{1}{2}} - 1\right]. \tag{41}$$

The lower bound on ζ when $B_L = \text{opt } B_L$ follows from the requirement that $\min \sigma_e{}^2 < \frac{1}{8}$ rad^2. Using (36) and some algebraic manipulation

$$\zeta^2 > \zeta_m{}^2 \equiv \frac{8k_rR^2}{\tau_{ce} - 32k_rR^2}, \tag{42}$$

which is a finite real lower bound on ζ only when the basic requirement (38) is satisfied.

Since ζ varies with range, the upper and lower bounds given above should be evaluated at the same range, R. It is apparent from (41) and (42) that the least upper bound and the greatest lower bound on ζ both occur at $R = R_{\max}$, and that the bounds constrict the range of ζ as the noise index, k_r, increases. As k_r decreases, the limits separate, allowing a wide range of ζ. However, from the point of view of relative stability and fast transient response, ζ should not be less than 0.7 nor greater than about two; also, from the point of view of minimizing $\sigma_e{}^2$,

it can be seen from (36) that there is negligible improvement in increasing ζ beyond about two. These restrictions on the range of ζ in the optimum design of the phase-lock loop can be summarized by

$$\max (0.7, \zeta_m) < \zeta \leqq \min (2.0, \zeta_M) \tag{43}$$

where ζ_M and ζ_m are the upper and lower bounds defined in (41) and (42), respectively.

Assuming that the set of positive real values of ζ satisfying (43) is not empty, the optimum choice of ζ (with respect to minimizing the mean-square phase error) is the least upper bound value given in (43). Using this value, the optimum value of the loop noise bandwidth, B_L, at maximum range is determined from (37) or Fig. 7.

The selection of the optimum ζ and B_L at maximum range fixes the value of the loop filter time constant, $\tau = R_2C$, as

$$\tau = \frac{4\zeta_{\text{opt}}^2 + 1}{4(B_L)_{\text{opt}}} = \begin{cases} T_M/4 , & \zeta_{\text{opt}} = \zeta_M \\ \dfrac{4.25}{(B_L)_{\text{opt}}} , & \zeta_{\text{opt}} = 2 \end{cases} \tag{44}$$

and the value of loop gain at maximum range as:

$$\alpha_{\min} K = \frac{4\zeta_{\text{opt}}^2}{\tau^2} . \tag{45}$$

When the IF bandwidth is specified, $\alpha_{\min}$ is determined from Fig. 11 in Appendix A, with $R = R_{\max}$. Knowing $\alpha_{\min}$, the loop gain constant, K, is then determined from (45). Since K has the lower bound given by (33) and certainly an upper bound dictated by practical equipment considerations, the range of α may have to be controlled through the selection of B_{IF} to give a value of K which is compatible with these bounds.

VI. *TELSTAR* SYSTEM DESIGN EXAMPLES

To illustrate this design approach, sample designs will be considered for both the precision tracker and the autotrack systems for the Telstar experimental program. Based on analysis of the expected orbit (see Appendix C), and on preliminary system data, the system parameters assumed for the design examples are given in Table I. While the IF bandwidth values are not necessarily fixed, the 200-kc bandwidth given in Table I for the 5-mc channels (see Fig. 2) is desirable from practical considerations.

Considering first the dynamic tracking capability in the absence of

TABLE I—ASSUMED SYSTEM PARAMETERS FOR DESIGN EXAMPLES

Equivalent coherence time, $\tau_{ce} = 0.02$ sec
Receiver noise index (see Section V)
PT system..... $k_r = 1.5 \times 10^{-5}$ sec/knm (kilo-nautical miles)
AT system..... $k_r = 2.0 \times 10^{-6}$ sec/knm
Orbital data:
Maximum range, $R_{max} = 5$ knm
Minimum range, $R_{min} = 0.5$ knm
Maximum Doppler shift, $|\Delta f| \doteq 100$ kc
Maximum rate of shift, $|\dot{\omega}| = 5620$ rad/sec^2, at 0.5 knm
IF bandwidth preceding limiter, $B_{IF} = 200$ kc (both systems)
Nominal range of loop gain constant, $K = 10^5$ to 10^6 sec^{-2}
Maximum tolerable settling time, $T_M = 0.1$ sec

noise, the dynamic range of the voltage-controlled oscillator in the phase-lock loop should be about ± 150 kc to avoid saturation effects when the maximum Doppler shift is ± 100 kc, and to allow for some drift of the center frequency during operation.

The range of variation of the limiter suppression factor, α, can be determined from Fig. 11 in Appendix A, using the values of k_r, R, and B_{IF} in Table I

	Precision Tracker	Auto-track
Max. range, $\alpha = \alpha_{min}$:	0.10	0.28
Min. range, $\alpha = \alpha_{max}$:	0.79	0.97

Since the maximum Doppler rate occurs at minimum range, the condition (33) that the maximum steady-state error be less than $\pi/6$ radian requires that the loop gain constant, K, satisfy

$$K > \frac{2 \times 5620}{\alpha_{max}} = \begin{cases} 1.42 \times 10^4 & \text{Precision Tracker} \\ 1.15 \times 10^4 & \text{Autotrack} \end{cases}$$

Both of these lower limits are well below the lower nominal value of 10^5 sec^{-2} given in Table I. Using this lower nominal value the maximum steady-state error in tracking the Doppler shift will be less than 0.08 radian for both systems [see (50), Appendix B].

The upper and lower bounds on ζ at maximum range condition, using (43) and Table I, are

Precision Tracker	Autotrack
$\left.\begin{matrix} 0.61 \\ 0.70 \end{matrix}\right\} < \zeta \leqq \left\{\begin{matrix} 1.76 \\ 2.0 \end{matrix}\right.$	$\left.\begin{matrix} 0.15 \\ 0.70 \end{matrix}\right\} < \zeta \leqq \left\{\begin{matrix} 2.95 \\ 2.0 \end{matrix}\right.$.

Taking the least upper bound as the optimum value gives at $R = R_{max}$

Precision Tracker	Autotrack
$\zeta_{opt} = 1.76$	$\zeta_{opt} = 2.0$

The min σ_e^2 and optimum B_L at maximum range, using (36) and (37) and the above values of ζ_{opt}, are

min $\sigma_e^2 = 0.1$ rad^2	min $\sigma_e^2 = 0.036$ rad^2
opt $B_L = 135$ cps	opt $B_L = 364$ cps.

Finally, using (44) and (45) and the values of α_{min} given above for the 200-kc IF bandwidth, the optimum values for the phase-lock loop constants τ and K are

$\tau = 0.025$ sec	$\tau = 0.012$ sec
$K = 2 \times 10^5$ sec^{-2}	$K = 4 \times 10^5$ sec^{-2}.

Since both values of K are greater than the lower bounds given above and are within the nominal range given in Table I, the desired 200-kc bandwidth need not be changed.

The performance of the systems as a function of the range, R, using these design parameters, is summarized by the curves shown in Figs. 8 and 9. These curves show how the input adaptive loop gain, αK, helps provide near-optimum design at ranges other than the maximum range where the optimum design was accomplished.

The mean-square phase error obtained from this linear analysis was compared with values obtained from the more accurate digital computer simulation of the phase-lock loop described in a separate paper.[9] Results for the two design examples considered above, which are shown in Fig. 10, demonstrate that although the error in the linear model estimate increased somewhat as the signal-to-noise ratio decreases, there is no drastic breakdown in the accuracy of the linear model. For these and two other designs tested, the linear analysis estimate of the threshold signal-to-noise ratio was within 1.5 db of the digital computer results.

VII. CONCLUDING REMARKS

The material presented in this paper was part of a design study conducted during the initial construction of the ground station tracking systems for the Telstar program. At that time there was some concern about the capability of the angle-error detector to maintain phase-lock at the longer satellite ranges, due to the small beacon signal power available and the uncertainty about the coherence time of the 4080-mc

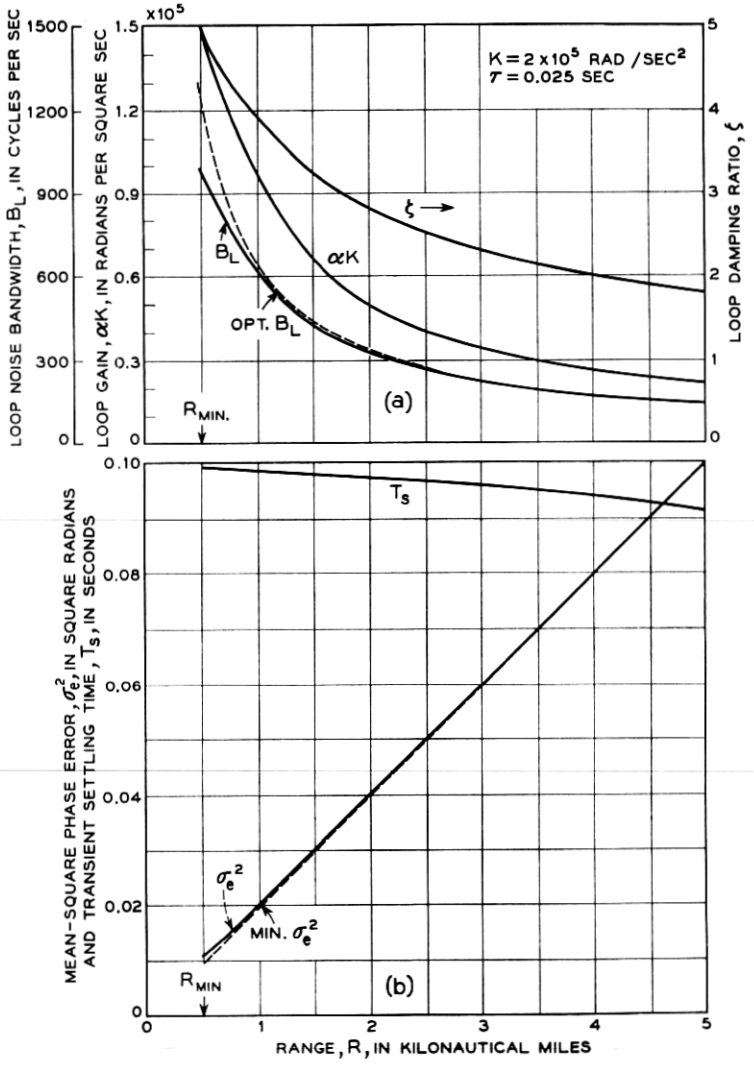

Fig. 8 — Performance curves for precision tracker (PT) optimum design example: (a) phase-lock loop parameter variations with range from ground station to satellite; (b) phase-lock loop performance measures as a function of range.

beacon signal. This was particularly critical in the detection system for the precision tracker because of the significantly lower gain of the precision tracker antenna compared to the horn-reflector antenna. For this reason, the means for achieving optimum design of the phase-lock

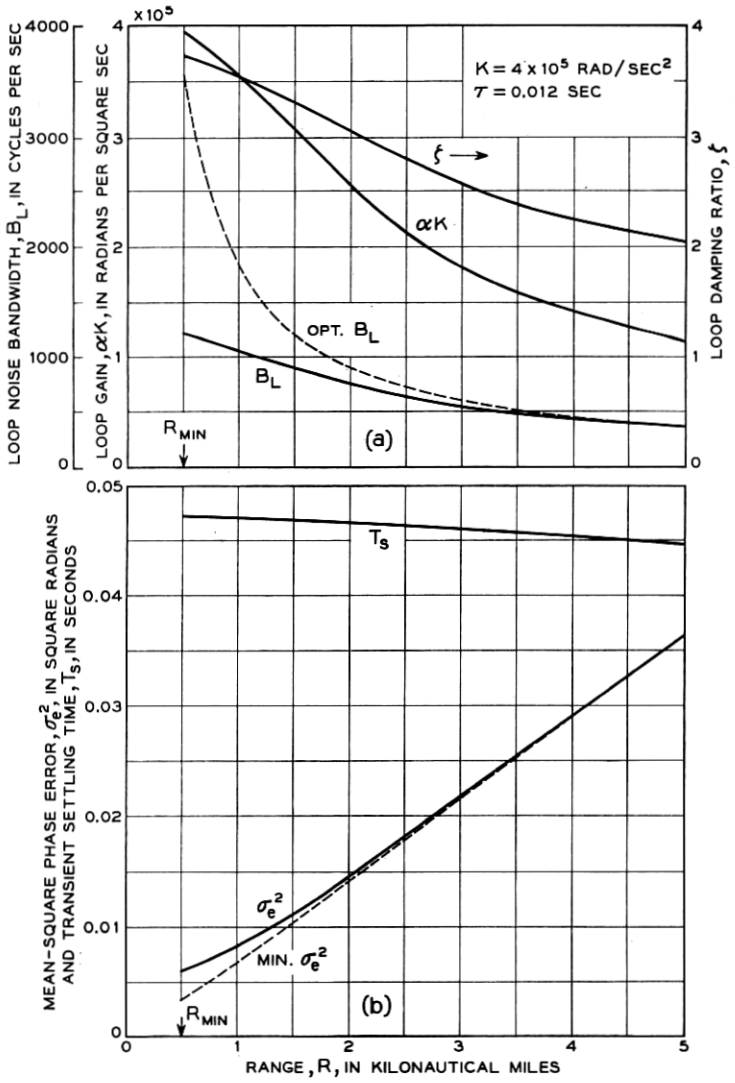

Fig. 9 — Performance curves for autotrack optimum design example: (a) phase-lock loop parameter variations with range from ground station to satellite; (b) phase-lock loop performance measures as a function of range.

loop at maximum range was a crucial consideration in the initial design. One of the fortunate results contributing to the highly successful operation of the first Telstar satellite experiment was the excellent phase stability achieved in the satellite beacon transmitter. Measurements of the mean-square phase error under strong-signal conditions

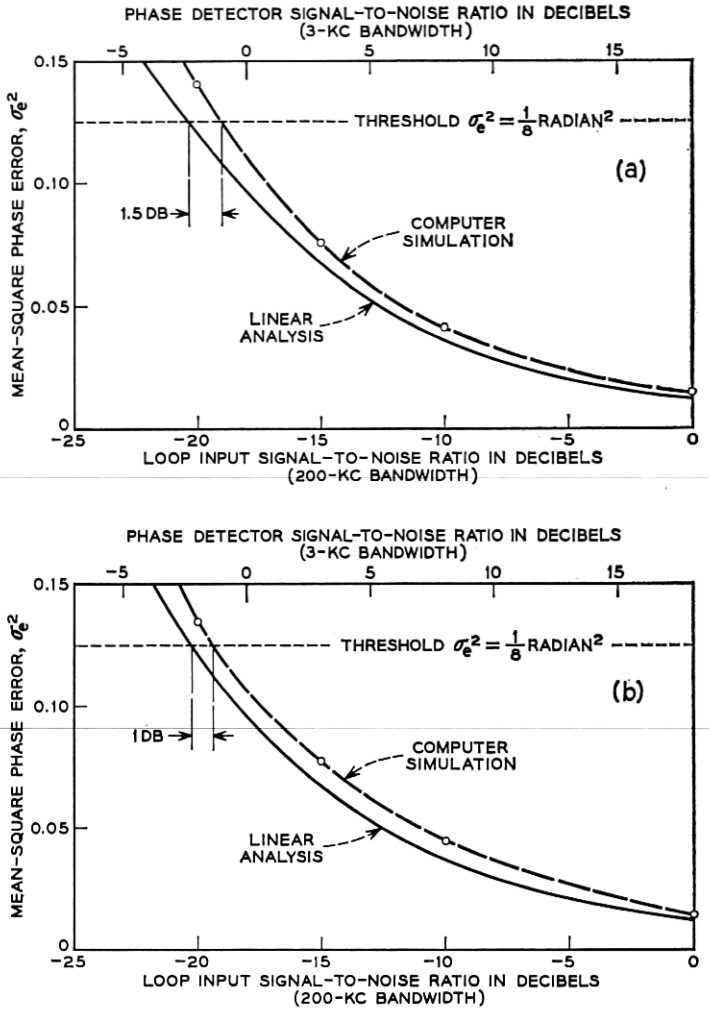

Fig. 10 — Comparison of mean-square error predicted by linear analysis with results from digital computer simulation of phase-lock loop, using design values from the two examples in Section VI.

(where the major contribution to the error is due to phase jitter in the beacon signal) indicated an effective coherence time of about 0.1 second instead of the 0.02-second value assumed for the design examples above. This higher coherence time makes the noise bandwidth and damping ratio adjustment in the phase-lock loop much less critical, as can be seen from the threshold contours in Fig. 7.

More detailed descriptions of the final design and the performance of the tracking systems in the first Telstar experiments are given in a series of papers [1,2,3] appearing in an earlier issue of this journal.

APPENDIX A

Effective Gain of Bandpass Limiter

Two factors which characterize the operation of an ideal bandpass limiter are:

(*i*) The total power output of the limiter remains constant,[11] i.e.

$$S_0 + N_0 = C \tag{46}$$

where S_0 = output signal power, N_0 = output noise power.

(*ii*) When a sinusoidal signal and narrow-band Gaussian noise are applied to the input of a bandpass limiter, the output signal to noise ratio is related to the input signal to noise ratio by[13]

$$\frac{S_0}{N_0} = \lambda \frac{S_i}{N_i} \tag{47}$$

where the factor λ, given in Fig. 5 of Ref. 13, varies from $\pi/4$ to 2 as the input signal to noise ratio varies from zero to infinity.

When no noise is present, we assume that the output signal power equals the input signal power (any fixed gain in the bandpass limiter is absorbed into the loop gain constant, K). Then, from (46), when $N_0 = 0$

$$S_0 = C = S_i$$

so that, when noise is present

$$S_0 + N_0 = S_i .$$

A little algebraic manipulation of this expression gives

$$\frac{S_0}{S_i} = \frac{\dfrac{S_0}{N_0}}{1 + \dfrac{S_0}{N_0}} .$$

Using (47), we obtain

$$\frac{S_0}{S_i} = \frac{\lambda \dfrac{S_i}{N_i}}{1 + \lambda \dfrac{S_i}{N_i}} \equiv \alpha^2 , \tag{48}$$

where α is called the limiter suppression factor.[11]

Thus, the limiter has the effect of reducing the signal power from S to $\alpha^2 S$, and as a consequence the effective loop gain is reduced from K to αK. The factor α defined in (48) varies from 0 to 1 as the input signal-to-noise ratio varies from 0 to ∞. From (30) in Section V, the input signal-to-noise ratio can be expressed as

$$\frac{S_i}{N_i} = (k_r R^2 B_{IF})^{-1} .$$

Using this expression in (48) gives

$$\alpha = \left[1 + \frac{k_r R^2 B_{IF}}{\lambda}\right]^{-\frac{1}{2}} ,$$

which shows the inverse dependence of α on the satellite range, R. With values of λ obtained from Fig. 5 of Ref. 13, the limiter suppression factor, α, is plotted as a function of the input signal-to-noise ratio in Fig. 11.

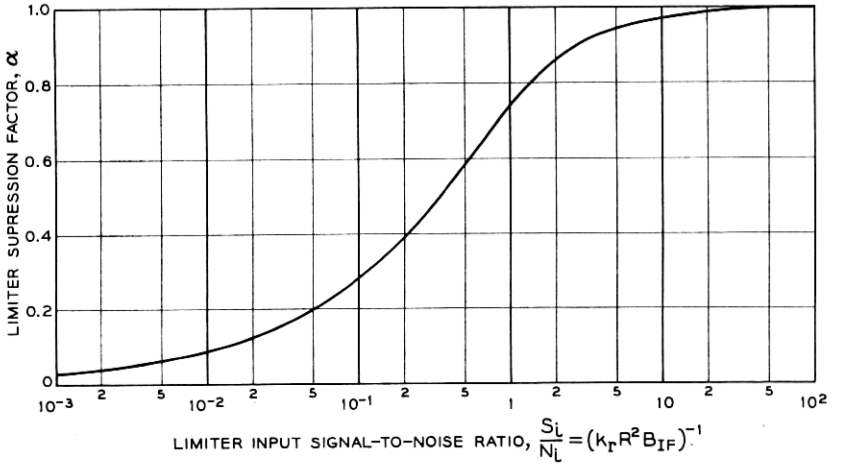

Fig. 11 — Limiter suppression factor, α, as a function limiter input signal-to-noise ratio.

APPENDIX B

Nonlinear Analysis of the Phase-Lock Loop

The phase-lock loop equivalent circuit, which includes the sine-function nonlinearity of the phase detector, is shown in Fig. 6(a). In terms of the phase error, θ_e, and its time derivative, ω_e, the differential equations governing the response of this circuit to the frequency-ramp input, $\omega_i = \dot{\omega}t$, are

$$\begin{aligned} \frac{d\theta_e}{dt} &= \omega_e \\ \frac{d\omega_e}{dt} &= \dot{\omega} - 2\zeta\omega_n\omega_e \cos\theta_e - \omega_n^2 \sin\theta_e \end{aligned} \tag{49}$$

where, as in Section IV, we define $\omega_n^2 \equiv \alpha K$, $2\zeta \equiv \tau\omega_n$.

The values of θ_e and ω_e which satisfy the equilibrium condition that the right-hand side of (49) vanish are

$$(\theta_e)_{eq} = \sin^{-1}\left(\frac{\dot{\omega}}{\alpha K}\right), \qquad (\omega_e)_{eq} = 0. \tag{50}$$

If the phase-lock loop "locks-on" to the frequency ramp input, the frequency error is zero, but there is a steady-state phase error given by equilibrium value in (50). A *necessary* condition for the existence of this phase-locked response is that

$$\alpha K > \dot{\omega}$$

i.e., the total loop gain must exceed the input frequency rate.

To analyze further the response of this circuit, it is convenient to normalize (49) in time and frequency with respect to the parameter ω_n. Defining the symbols

$$\begin{aligned} x &\equiv \omega_n t \\ \nu &= \omega_e/\omega_n \\ r &= \dot{\omega}/\omega_n^2 = \dot{\omega}/\alpha K \end{aligned}$$

the differential equation (49) can be written.

$$\begin{aligned} \frac{d\theta}{dx} &= \nu \\ \frac{d\nu}{dx} &= r - 2\zeta\nu \cos\theta - \sin\theta \end{aligned} \tag{51}$$

where $\theta \equiv \theta_e(t)$ is assumed in the remainder of Appendix B.

The solutions of these equations for given initial conditions and given value of normalized input rate, r, describe trajectories in the normalized (θ, ν) state space. The slope of these trajectories in this state space is, from (51)

$$\frac{d\nu}{d\theta} = \frac{r - \sin\theta}{\nu} - 2\zeta\cos\theta. \tag{52}$$

For initial conditions $\theta = 0$, $\nu = 0$ (corresponding to the circuit being in steady-state phase lock with constant frequency input prior to the onset of the frequency-ramp input), two sets of trajectories obtained from numerical integration of (52) are shown in Fig. 12. In Fig. 12(a) a value of $r = 0.966$ is chosen to illustrate the response when the loop gain exceeds the frequency rate only slightly. It can be seen that for $\zeta \geqq 1$, the phase error tends to the steady-state value of 1.31 radians ($= \sin^{-1} 0.966$) with only small overshoot. For $\zeta = 0.707$, however, there is a large overshoot which actually exceeds $\pi/2$ radians, but eventually returns to the steady-state value; for $\zeta < 0.707$ the phase error does not reach the steady-state: i.e., the circuit is unable to "lock-on."

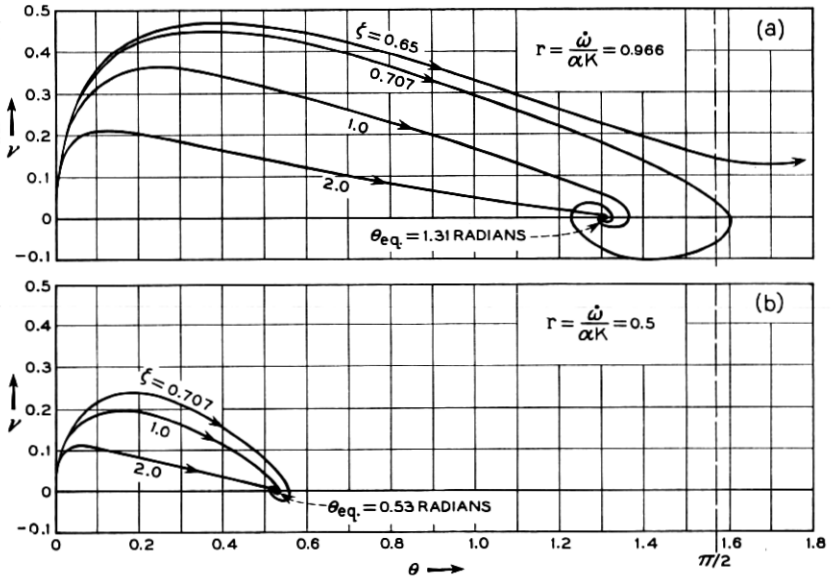

Fig. 12 — Trajectories of the phase-lock loop response to frequency ramp input for various values of the damping ratio: (a) input frequency rate, $\dot{\omega}$, nearly equal to the loop gain, αK; (b) input frequency rate, $\dot{\omega}$, equal to one-half the loop gain, αK.

To avoid large steady-state phase errors and large peak phase errors with the attendant likelihood of random perturbations causing the circuit to fall out of phase lock, the following conditions should be imposed

$$\left.\begin{aligned} \alpha K &\geqq 2\dot{\omega} \\ \zeta &> 0.7 \end{aligned}\right\}. \tag{53}$$

Fig. 12(b) shows a set of trajectories with conditions (53) satisfied. The response closely approximates that of the linear second-order system obtained by letting $\sin \theta = \theta$, $\cos \theta = 1$ in (51).

APPENDIX C

Satellite Orbit Characteristics

The parameters of the satellite orbit which affect the design of the phase-lock loop are evaluated in this appendix. The effect of the oblateness of the earth and other perturbations upon the satellite orbit is neglected in this analysis. However, since this effect does cause rotation of the perigee, the maximum range, minimum range and maximum Doppler effects are derived considering all possible locations of the perigee relative to the ground station.

The geometry and terminology of the analysis is shown in Fig. 13(a). It is sufficient to consider only the condition when the ground station is in the plane of the orbit in order to derive all the parameters needed.

(*i*) *Minimum and Maximum Communicating Range.* It is obvious that the minimum possible range occurs when the satellite passes overhead at perigee. Therefore

$$R_{\min} = R_p = \text{perigee altitude.} \tag{54}$$

From the point of view of the satellite, the maximum possible range to any visible point on earth occurs when the satellite is at apogee and the range is taken along the tangent to the earth's surface. The satellite would then appear on the horizon at maximum range to a tracking station anywhere along the locus of these points of tangency.

Since, however, the satellite must be at a small angle, φ_h, above the horizon before communication is feasible at maximum range, the conditions at the maximum possible communication range are as shown in Fig. 13(b). In terms of the angle φ_c in Fig. 13(b)

$$R_{\max}^2 = r_a^2 + r_0^2 - 2r_a r_0 \cos \varphi_c$$

where

r_0 = radius of earth

$r_a = R_a + r_0$, R_a = apogee altitude.

Now for φ_h small (less than about 10°), the angle φ_c is very closely given

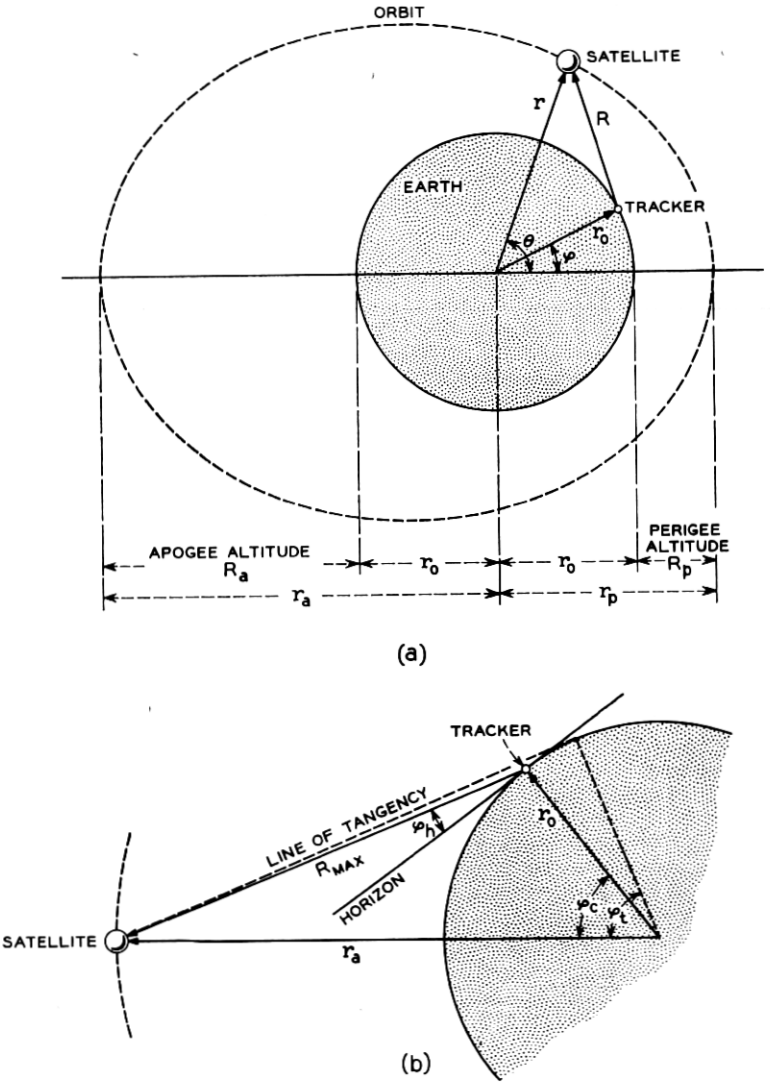

Fig. 13 — Satellite orbit diagrams: (a) geometry and terminology for satellite orbit; (b) conditions for maximum communication range.

by

$$\varphi_c \doteq \varphi_t - \varphi_h, \qquad \varphi_t = \cos^{-1}\left(\frac{r_0}{r_a}\right).$$

Therefore, in terms of known parameters and a given horizon angle φ_h, the maximum possible communication range is

$$R_{\max} \doteq [r_a^2 + r_0^2 - 2r_a r_0 \cos(\varphi_t - \varphi_h)]^{\frac{1}{2}} \tag{55}$$

where

$$\varphi_t = \cos^{-1}(r_0/r_a).$$

(ii) Maximum Doppler Shift and Rate. The orbit parameters needed to determine these Doppler effects are the maximum range rate, $\dot{R}_{\max}$, and the maximum range acceleration, $\ddot{R}_{\max}$. The parametric equation of the satellite orbit in polar form corresponding to the choice of coordinates in Fig. 13(a) is

$$r = \frac{r_m}{1 + \epsilon \cos\theta} \tag{56}$$

where

$$r_m = \frac{2r_a r_p}{r_a + r_p}$$

$$\epsilon = \frac{r_a - r_p}{r_a + r_p} = \text{eccentricity of orbit}$$

$$r_a = R_a + r_0$$

$$r_p = R_p + r_0.$$

Furthermore, from the "law of areas" for motion in a central force field

$$\dot{\theta} = \frac{k}{r^2} \text{ rad/sec} \tag{57}$$

where

$$k^2 = GMr_m = gr_0^2 r_m$$

G = universal gravitational constant

M = mass of earth

g = acceleration due to gravity at surface of earth.

From Fig. 13(a), the range, R, for a tracker at angle φ is related to the orbit variables, r and θ, by

$$R^2 = r^2 + r_0^2 - 2r_0 r \cos(\theta - \varphi). \tag{58}$$

Differentiating this expression and using (57) gives for the range rate $\dot{R}$

$$\dot{R} = \frac{\dot{r}}{R}[r - r_0 \cos(\theta - \varphi] + \frac{kr_0}{Rr} \sin(\theta - \varphi) \tag{59}$$

and for the range acceleration, $\ddot{R}$

$$\ddot{R} = \frac{\ddot{r}}{R}[r - r_0 \cos(\theta - \varphi)] + \frac{\dot{r}^2 - \dot{R}^2}{R} + \frac{k^2 r_0}{Rr^3} \cos(\theta - \varphi). \tag{60}$$

These expressions depend upon r, $\dot{r}$, and $\ddot{r}$, which are determined as a function of θ by the orbit equations (56) and (57). The evaluation of $\dot{R}_{\max}$ is rather tedious and is most easily obtained for a given orbit by machine or graphical computation. It was evaluated for the expected Telstar satellite orbit using a part graphical and part analytical computation, with the results given at the end of this appendix.

The evaluation of $\ddot{R}_{\max}$ is quite easily obtained, however, since it occurs for the conditions $\theta = \varphi = 0$; i.e., when the satellite passes overhead at perigee. The maximum range acceleration is given by

$$\ddot{R}_{\max} = g \frac{r_0^2}{(R_p + r_0)^2}\left(\frac{r_m}{R_p} - 1\right) \tag{61}$$

which occurs when $R = R_{\min} = R_p$.

The maximum Doppler rate varies directly with the maximum range acceleration

$$\dot{\omega}_{\max} = \frac{2\pi f_b}{c} \ddot{R}_{\max} = 2\pi f_b \frac{g}{c}\left[\frac{r_0^2}{(R_p + r_0)^2}\left(\frac{r_m}{R_p} - 1\right)\right] \tag{62}$$

where

f_b = satellite beacon frequency

c = velocity of light.

To estimate the maximum Doppler rate which might be expected for practical communication satellite systems, we take the following conditions as representing practical extremes from the point of view of good communication and satellite lifetime

$$\text{maximum } f_b = 5 \times 10^9 \text{ cyc/sec}$$

$$\text{minimum perigee, } R_p = 0.2 \text{ knm}$$

$$\text{maximum apogee, } R_a = 5.0 \text{ knm}.$$

Using these values in (62) gives as an estimate for the maximum expected Doppler rate

$$\max\ (\dot{\omega}_{\max}) \approx 2 \times 10^4 \text{ rad/sec}^2.$$

(iii) Numerical Values for the Expected Telstar Satellite. The constants needed for the range and Doppler calculations are:

$$R_p = 0.5 \text{ knm (perigee)}$$

$$R_a = 3.0 \text{ knm (apogee)}$$

$$r_0 = 3.44 \text{ knm}$$

$$r_m = 4.88 \text{ knm}$$

$$g/c = 3.27 \times 10^{-8} \text{ sec}^{-1}; \qquad c = 162 \text{ knm/sec}$$

$$f_b = 4.08 \times 10^9 \text{ cyc/sec}$$

$$\varphi_h = 7.5° \text{ (acquisition angle above horizon)}.$$

Using these numerical constants in (54), (55), and (62) gives for $R_{\min}$, $R_{\max}$, and $\dot{\omega}_{\max}$ the values:

$$R_{\min} = 0.5 \text{ knm}$$

$$R_{\max} = 5.0 \text{ knm}$$

$$\dot{\omega}_{\max} = 5.62 \times 10^3 \text{ rad/sec}^2.$$

The maximum value of $\dot{R}$ in (59) for the Telstar satellite orbit was found to occur when $\theta = 340°$, $\varphi = 10°$ and has a magnitude

$$|\dot{R}|_{\max} \doteq 4 \times 10^{-3} \text{ knm/sec}.$$

The maximum Doppler shift is then given by

$$|\Delta f|_{\max} = \frac{f_b}{c} |\dot{R}|_{\max} \doteq 100 \text{ kc}.$$

REFERENCES

1. Githens, J. A., Kelly, H. P., Lozier, J. C., and Lundstrom, A. A., Antenna Pointing System: Organization and Performance, B.S.T.J., **42**, July, 1963, p. 1213.
2. Anders, J. V., Higgins, E. F., Murray, J. L., and Schaefer, F. J., The Precision Tracker, B.S.T.J., **42**, July, 1963, p. 1309.
3. Cook, J. S., and Lowell, R., The Autotrack System, B.S.T.J., **42**, July, 1963, p. 1283.
4. Develet, J. A., Jr., Fundamental Sensitivity Limitations for Second-Order Phase-Lock Loops, STL Report 8616-0002-NU-000, June 1, 1961.

5. Develet, J. A., Jr., Thermal Noise Errors in Simultaneous Lobing and Conical Scan Angle-Tracking Systems, I.R.E. Trans. on Space Electronics and Telemetry, **SET 7,** June, 1961, pp. 42-51.
6. Jaffe, R., and Rechtin, E., Design and Performance of Phase-Lock Circuits Capable of Near-Optimum Performance Over a Wide Range of Input Signal and Noise Level, I.R.E. Trans. Inf. Theory, **IT 1,** March, 1955, pp. 66–76.
7. James, H. M., Nichols, N. B., and Phillips, R. S., *Theory of Servomechanisms*, Rad. Lab. Series, **25,** McGraw-Hill, New York, 1947, pp. 369–370.
8. Enloe, L. H., unpublished work.
9. Ball, W. H. W., Analysis and Digital Simulation of the *Telstar* Precision Tracker, Paper No. CP-63-368, presented at the IEEE Winter General Meeting, New York, 1963.
10. D'Azzo, J. J., and Houpis, C. H., *Control System Analysis and Synthesis*, McGraw-Hill, New York, 1960, pp. 58–62.
11. Viterbi, A. J., System Design Criteria for Space Television, J. Brit. I.R.E., **19,** Sept., 1959, pp. 561–570.
12. Brockman, M. H., Buchanan, H. R., Choate, R. L., and Malling, L. R., Extra-Terrestrial Radio Tracking and Communication, Proc. I.R.E., **48,** No. 4, April, 1960, pp. 643–654.
13. Davenport, W. B., Jr., Signal-to-Noise Ratios in Band-Pass Limiters, J. Appl. Phys., **24,** June, 1953, pp. 720–727.